Showcasing research from Sankarasekaran Shanmugaraju's laboratory, Department of Chemistry, Indian Institute of Technology Palakkad, Kerala, India.

Recent advances in fluorescence-based chemosensing of organoarsenic feed additives using luminescence MOFs, COFs, HOFs, and QDs

Organoarsenics are low-toxicity compounds that are used widely as feed additives to promote livestock growth, enhance meat pigmentation, and fight against intestinal parasites. The degradation of organoarsenic produces toxic carcinogen inorganic arsenic such as As(v) and As(III), which results in severe arsenic pollution of soil and groundwater. This article highlights various fluorescence chemosensors reported to date for sensing organoarsenic feed additives.

ROYAL SOCIETY
OF **CHEMISTRY**

rsc.li/chemcomm

Registered charity number: 207890

Check for updates

Recent advances in fluorescence-based chemosensing of organoarsenic feed additives using luminescence MOFs, COFs, HOFs, and QDs

Rajdeep Mondal,†[a] Ananthu Shanmughan, 🆔†[a] A. Murugeswari*[ab] and Sankarasekaran Shanmugaraju 🆔*[a]

Organoarsenics are low-toxicity compounds that are used widely as feed additives to promote livestock growth, enhance meat pigmentation, and fight against intestinal parasites. The organoarsenic compounds are commonly found in poultry waste and the degradation of organoarsenic produces the toxic carcinogen inorganic arsenic such as As(v) and As(III), which results in severe arsenic pollution of soil and groundwater. As a consequence, there exists a high necessity to develop suitable sensing methods for the trace detection and quantification of organoarsenic feed additives in wastewater. Among various detection methods, in particular, fluorescence-based sensing has become a popular and efficient method used extensively for sensing water contaminants and environmental contaminants. In the recent past, a wide variety of fluorescence chemosensors have been designed and employed for the efficient sensing and quantification of the concentration of organoarsenic feed additives in different environmental samples. This review article systematically highlights various fluorescence chemosensors reported to date for fluorescence-based sensing of organoarsenic feed additives. The fluorescence sensors discussed in this review are classified and grouped according to their structures and functions, and in each section, we provide a detailed report on the structure, photophysics, and fluorescence sensing properties of different chemosensors. Lastly, the future perspectives on the design and development of practically useful sensor systems for selective and discriminative sensing of organoarsenic compounds have been stated.

[a] *Department of Chemistry, Indian Institute of Technology Palakkad, Palakkad 678557, Kerala, India. E-mail: shanmugam@iitpkd.ac.in*

[b] *Department of Physics, Anna University, Chennai 600025, India. E-mail: murugeswari@annauniv.edu*

† These authors contributed equally.

1. Introduction

In the year 1907 Bertheim in Paul Ehrlich's lab invented the first chemotherapeutic drug Arsphenamine, which was used to treat syphilis, a scourge that affected a significant proportion of

Mr Rajdeep Mondal completed his MSc from the Indian Institute of Technology Palakkad, Kerala, India. He received his BSc degree from Kazi Nazrul University, West Bengal, India. His current research interests are in supramolecular chemistry and sensor chemistry.

Rajdeep Mondal

Mr Ananthu Shanmughan is currently a PhD student at the Indian Institute of Technology Palakkad. He has completed his Integrated MSc in Chemistry from IIRBS, Mahatma Gandhi University, Kottayam. His current research interests include designing and developing small-molecule fluorescence sensors and the synthesis of luminescent organic polymers for the sensing of emerging organic pollutants.
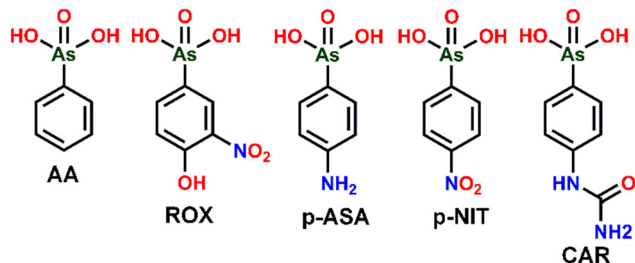
Ananthu Shanmughan

Fig. 1 The structure of representative organoarsenic feed additives is discussed in this article.

men and women in the early 20th century.[1,2] Bertheim and team on their search for a magic bullet that selectively kills the microbes, came across a compound called compound-606, later known by its trade name Salvarsan was the first organic antisphylitic.[3] It later paved the way for many other structurally related arsenicals for various medical applications. Roxarsone (ROX, 3-nitro-4-hydroxyphenylarsonic acid) was one of those compounds that were used to control cecal coccidiosis in poultry.[4,5] On further investigation ROX was also found to have therapeutic activities like growth promoter, improvement of feed conversion, increased egg production and pigmentation, etc. This led to the rise of many other structurally similar organoarsenic compounds like phenylarsonic acid (AA), p-arsanilic acid (p-ASA, 4-aminophenylarsonic acid), nitarsone (p-NIT, 4-nitrophenylarsonic acid), and carbarsone (CAR, p-ureidophenylarsonic acid) (see Fig. 1 for structures). Among various organoarsenics, ROX and p-ASA are used extensively as additives to animal feeds for their applications in disease prevention and growth promotion effects in poultry and swine production.[5,6]

Organoarsenics are significantly less toxic compounds compared to inorganic arsenicals, As(v) and As(III), whose health problems due to their long-term exposure are thoroughly investigated and classified as a carcinogen in 1980 that can cause serious disturbances to the cardiovascular and central nervous systems.[7,8] Although reports are suggesting that organoarsenic feed additives are toxic if supplemented at a higher dosage than recommended levels, until the early 2000's, there was no special attention given to the fate of organoarsenic feed additives in the environment and very little was known about their metabolic processes.[8,9] There are no shreds of evidence confirming that long-term exposure to organoarsenics is carcinogenic.[9] It has been observed that organoarsenic compounds cannot be completely digested by animals and are mostly excreted as urine and faeces. The excreta of animals that contain organoarsenic is applied as manure in agricultural lands leading to the accumulation of high concentrations of organoarsenic content in the soil. Once entered into the soil, these feed additives can break down into various products such as arsenite (As(III)), arsenate (As(v)), dimethylarsinate (DMA), monomethylarsonate (MMA), 3-amino-4-hydroxarsoneyphenylarsonicacid (HAPA), and other As species through biotic and abiotic action.[10,11]

In addition to these arsenical residues, either metabolized or non-metabolized will remain in the tissues of poultry or swine. Studies by Lasky et al., in 2004 and Nachman et al., in 2017 revealed that poultry fed with feed additives had an increased level of inorganic arsenic in their liver compared to that of control.[12,13] This also increases the possibility of inorganic arsenic intake by humans through meat. Mondal et al., in 2020 conducted a study that estimated the levels of arsenic contamination in the flesh of different body parts of poultry chicken in West Bengal. According to the results obtained, the consumption of inorganic arsenic even when a person has an average of 60 g of chicken every day will be less than the permissible level (~ 10 ppb) of inorganic arsenic intake set by the World Health Organization (WHO).[14] Although arsenic in animal tissues was generally lower than the tolerance level given by WHO (0.5 mg kg^{-1}), the total arsenic (As) and inorganic arsenic (i-As) in phenylarsonic-fed animal tissues

Dr A. Murugeswari is working as an Assistant Professor at Anna University, Chennai. She was awarded a PhD degree from the Bharathidasan University, Tiruchirappalli. Her current research interests include high-pressure physics, advanced magnetic materials, composites, solar cells, and chemosensors.

A. Murugeswari

Dr Sankarasekaran Shanmugaraju received his PhD degree with a gold medal for the best PhD thesis in Inorganic Chemistry from the Indian Institute of Science (IISc), Bengaluru. In 2014, he moved to Trinity College Dublin, Ireland as an Irish Research Council (IRC) postdoctoral fellow. In 2018, he joined the Indian Institute of Technology Palakkad (IITPKD) as an assistant professor. Since June 2023, he has been an associate professor at IITPKD.

Sankarasekaran Shanmugaraju

His current research activities are in the area of supramolecular materials and sensor chemistry.

were higher than those in non-fed animal tissues, indicating ROX could pose a risk to human health through environmental and animal food routes.[15–18]

Many countries have have taken initiatives to address the health and environmental risks posed by organoarsenic feed additives. Some countries have banned or phased out the use of organoarsenic feed additives. The European Union banned the use of ROX in 1999,[15] which prompted the US and Canada to suspend sales of ROX in 2011. In 2013, the Food and Drug Administration (FDA) withdrew approval for the use of p-ASA and CAR in food-producing animals, and in 2015, p-NIT was also withdrawn.[16,17] China also joined global efforts to phase out phenyl arsenic by banning the use of phenyl arsenic feed additives in 2019[18] after discovering that the concentration of As in compost sites of chicken farms was significantly higher than that in background soil.[19] However, many developing countries continue to use phenyl arsenic feed additives without proper regulation, leading to unchecked health risks. As these additives can degrade into i-As, developing suitable detection and removal methods for organoarsenic in the feed additives of poultry and swine farms is crucial. As a result, scientists have made enormous efforts in detecting organoarsenic in food and environmental samples by different sensitive detection methods.

Various analytical methods currently available for the detection of toxic analytes (including organoarsenics) includes liquid chromatography along with an atomic fluorescence spectrometry (LC-AFS),[20] liquid chromatography–mass spectrometry (LCMS),[21,22] high performance liquid chromatography (HPLC),[23] HPLC-inductively coupled plasma-mass spectrometry (HPLC-ICP-MS),[24] hydride generation atomic absorption spectrometry (HG-AAS),[25] hydride generation atomic fluorescence spectrometry (HG-AFS),[26,34] inductively coupled plasma mass spectrometry (ICP-MS),[27,28] inductively coupled plasma optical emission spectrometry (ICP-OES),[29] gas chromatography (GC),[30] gas chromatography-inductively coupled plasma mass spectrometry (GC-ICP-MS),[31] solid-phase extraction with a gas chromatography detector,[32] electrothermal atomic absorption spectrometry (ET-AAS),[33] total reflection X-ray fluorescence (XRF),[35] voltammetry,[36] spectrophotometry,[37,38] surface-enhanced Raman scattering,[39] electrochemical method,[40] capillary electrophoresis coupled with mass spectrometry,[41] and electroanalytic detection.[42] Although these instrument techniques show good sensitivity and efficiency but also have shortcomings. All these techniques require high costs for maintenance and require trained operators. It involves careful pre-treatment operations, effective separation methods, large solvent consumption, and time-consuming preparation, which are difficult when dealing with the analysis of large quantities of samples. Instruments are also non-portable which can limit their use in real-time routine monitoring of feed additives in wastewater. Therefore, a method, which can precisely detect feed additives with high selectivity, and sensitivity in real-time with simple operations and low cost is in high demand concerning environmental pollution.

Given this, in recent years, fluorescence-based sensing has become an efficient and promising detection method because

of the various advantages like high selectivity and superior sensitivity of detection, fast-response time, low cost, and simple operational procedure.[43,44] Until recently, a variety of fluorescence chemosensors have been developed and employed to efficiently sense organoarsenic feed additives even in a competitive sensing environment. The fluorescent sensors that have been developed over the years include metal–organic frameworks (MOFs), covalent organic frameworks (COFs), hydrogen-bonded organic frameworks (HOFs), and luminescence quantum dots (QDs). In this review article, we attempted to systematically elaborate on various fluorescent chemosensors reported to date for sensing organoarsenic feed additives. This review presents an overall picture of the current development in fluorescence-based sensing of organic feed additives and thus, this review will greatly benefit the researchers working in environmental and sensor chemistry. Also, this article will give inspiration for future studies to develop practically feasible fluorescence sensor systems. To the best of our knowledge, this is the first review article highlighting the recent advances in the use of various fluorescence sensors for organoarsenic detection. The following sections demonstrate the fluorescence sensing properties of different sensor materials and their mechanism of sensing towards organoarsenic feed additives.

2. Fluorescence-based sensing of organoarsenic feed additives

In recent years, fluorescence-based sensing has become a most promising and cost-effective sensing method for the detection of hazardous substances and environmental pollutants.[45] In fluorescence-based sensing, the sensor's initial fluorescence emission intensity is perturbed, either quenched or enhanced, upon interacting with target analytes.[46] It has been shown that the electron-deficient analytes adorned with electron-withdrawing groups like NO_2 quench the fluorescence emission intensity of sensors while the electron-rich analytes enhance the sensor's emission intensity.[47] The organoarsenic compounds are mostly electron-deficient and thus, the fluorescence emission intensity of sensors is quenched upon mixing the sensor solutions with organoarsenic analytes (see Fig. 2). The fluorescence quenching also due to the arsenic heavy atom effect.[48]

The fluorescence-quenching-based sensing can be either by the ground-state static mechanism or by an excited-state dynamic quenching mechanism operated via a simple electron-transfer process from the photoexcited sensor molecules, which acts as donor, to the analytes, which acts as acceptor.[49] These sensing mechanisms can be differentiated by measuring the lifetime of sensors before and after the addition of target analytes. If there are notable changes in the fluorescence lifetime of sensors, then the fluorescence quenching follows a static quenching mechanism via ground state complexation. In contrast, no changes in the lifetime of sensors indicate that the sensor binds with analytes in the excited state and follows a dynamic fluorescence quenching mechanism.[50]
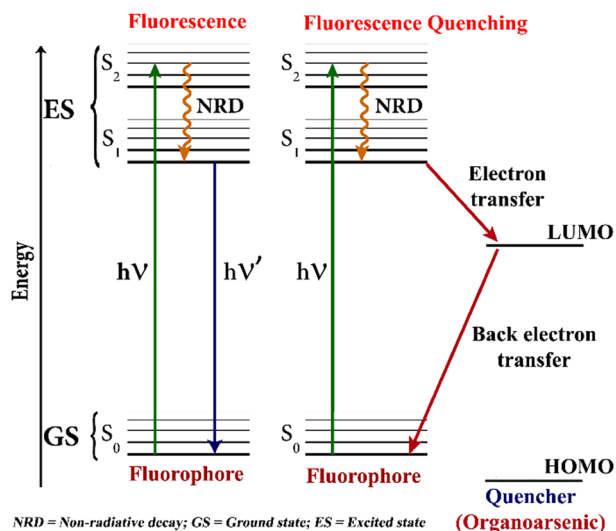
Fig. 2 A pictorial representation of the fluorescence quenching-based detection of organoarsenic feed additives using fluorescence chemosensors.

The static or dynamic quenching mechanisms give a linear Stern–Volmer curve and the Stern–Volmer quenching constant (K_{SV}) can be determined from the slope of the linear curve.[51] The higher value of K_{SV} indicates that sensor molecules strongly bind with the target analytes resulting in strong fluorescence quenching.[52,53] The following sections describe the structures, photophysics, and fluorescence sensing mechanisms of different kinds of fluorescence sensors for organoarsenic feed additives sensing.

3. Metal–organic frameworks (MOFs)-based fluorescence sensors

Metal–organic frameworks (MOFs) are an emerging class of crystalline porous polymers and they are synthesized *via* solvothermal reaction between metal ions or metal clusters and organic bridging ligands.[54] By the judicious choice of organic linkers, the surface and functional properties of MOFs can be modulated to meet the targeted applications.[55] In the past decades, MOFs have been heavily researched as emerging multi-functional porous material that has shown promising applications in gas storage, drug delivery, adsorption, catalysis, and sensing.[56,57] The promising properties like high surface area, high porosity, adjustable pore volume, and specific electric and optical properties make MOFs highly desirable materials that can encapsulate as well as identify the target guest molecules within their internal voids.[58] Among various classes of MOFs, in particular, luminescent MOFs (LMOFs) are fascinating for their potential applications in task-specific fluorescence sensing of toxic and hazardous pollutants.[59,60] In this section, several LMOFs-based fluorescent sensors already reported for efficient detection of organoarsenic feed additives are described.

In 2019, Su and coworkers reported the first LMOFs-based fluorescence sensors for organoarsenic detection.[61] Aluminium-based LMOFs have been used extensively in fluorescence sensing applications owing to their high stability, and interesting photoluminescence properties.[62] Given this, two chemically stable, isostructural luminescent Aluminium MOFs, BUT-18 {Al(CTTA)} and BUT-19 {Al(CETA)} were synthesized and employed as fluorescent chemosensors that can sense two representative organoarsenics such as ROX and *p*-NIT in water. The presence of electron-withdrawing NO_2 groups makes ROX and *p*-NIT electron-deficient in nature and strongly interacts with electron-rich LMOFs resulting in a significant fluorescence quenching.[63] BUT-18 was freshly prepared by hydrothermal reaction between $Al(NO_3)_3·9H_2O$ and dimethyl-5′-(4-(methoxycarbonyl)phenyl)-2′,4′,6′-trimethyl-[1,1′:3′,1″-terphenyl]-4,4″-dicarboxylic acid (H_3CTTA) dissolved in acetic acid and dimethylformamide (DMF), while BUT-19 was synthesized from dimethyl2′,4′,6′-triethyl-5′-(4-(methoxycarbonyl)phenyl)-[1,1′,3′,1″-terphenyl]-4,4″-dicarboxylic acid (H_3CETA), after heating the reaction mixture in DMF along with trace amount of formic acid (see Fig. 3(A) and (B) for the structure of organic linkers). Acetic acid or formic acid was used as a competing reagent during the solvothermal synthesis of LMOFs. The methyl groups in linker H_3CTTA and ethyl functionality in ligand H_3CETTA were introduced to increase hydrophobicity at the metal centers and thus, enhance the hydrolytic stability (stability in water) of frameworks. Both BUT-18 and BUT-19 consist of octahedral $[AlO_6]^-$ which form 1D chain-like building units through carboxylate coordination and these 1D chains were further connected by the tritopic aromatic linkers to form 3D frameworks with large hexagonal pore structures (Fig. 3(C)–(E)). Interestingly, the 3D frameworks were found to be hydrolytically more stable due to the presence of hydrophobic organic linkers and high valence metal ions, which prevents hydrolysis and framework degradation in water.[64]

BUT-18 and BUT-19 showed high surface area, moderate pore sizes, and good framework chemical stability in an aqueous solution of HCl (pH = 1) and NaOH (pH = 10). The fluorescence sensing studies of these LMOFs in water exhibited the highest quenching efficiency towards ROX and *p*-NIT, while other organoarsenics exhibited moderate to poor fluorescence quenching (Fig. 3(G)). The initial emission intensity of LMOFs was quenched drastically upon increasing the concentrations of ROX or *p*-NIT (Fig. 3(F)). The limit of detection (LoD) values of BUT-18 for ROX and *p*-NIT were determined to be 15.7 and 32.2 ppb, while BUT-19 exhibited 13.5 and 13.3 ppb, respectively. Notably, both BUT-18 and BUT-19 showed a preferential binding affinity for ROX and *p*-NIT even in the presence of other competing feed additives such as erythromycin, penicillin, thiamphenicol, and cypermethrin, which confirms their high selectivity (Fig. 3(G)). The computational calculations showed that the LUMO energy of analytes (ROX and *p*-NIT) is lower compared to the LUMO energy of sensors (BUT-18 and BUT-19) which confirms the possibility of photo-induced electron transfer (PET) from excited LMOFs to the analytes. Further, the significant spectral overlap between the absorption spectrum of the analyte and the emission spectra of LMOFs indicates the
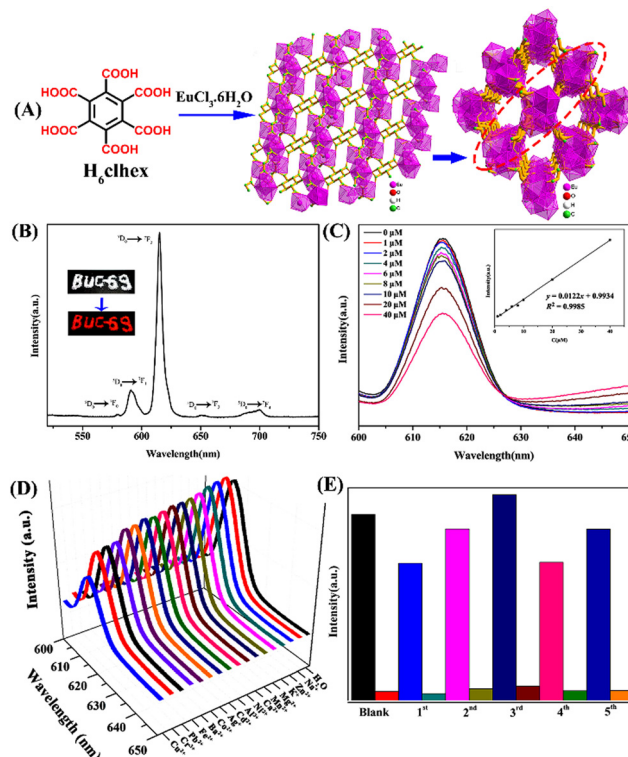
Fig. 3 The structure of organic linker (A) H_3CTTA and (B) H_3CETA. The framework structure of (C) BUT-18, (D) BUT-19, and (E) their 3D view of solid-state packing diagram. (F) The relative changes in fluorescence emission intensity for BUT-18 upon the addition of ROX in water. (G) The changes in emission intensity for BUT-18 and BUT-19 after the addition of different analytes. Reprinted with permission from ref. 61. Copyright 2019 Royal Society of Chemistry.

Fig. 4 (A) The structure of organic linker H_6clhex, 2D network, and 3D framework of BUC-69. (B) The solid-state fluorescence emission spectrum of BUC-69 was recorded at room temperature. (C) The changes in emission spectra of BUC-69 upon increasing the concentrations of p-ASA (inset: Stern–Volmer plot). (D) The emission spectra of BUC-69 were measured in the presence of different metal ions. (E) The recyclability test for reversible sensing of p-ASA. Reprinted with permission from ref. 65. Copyright 2019 Willey.

fluorescence resonance energy transfer (FRET) mechanism also contributes to observed fluorescence quenching. The fluorescence quenching responses of LMOFs were found to be reversible; the emission intensity of LMOFs remained unchanged even after six cycles of sensing studies. All these studies demonstrated that both BUT-18 and BUT-19 can be practically useful sensor systems for selective sensing of organoarsenics in water.

A stable Eu(III)-based 3D LMOF (BUC-69) was synthesized that can selectively sense the presence of p-ASA in water.[65] p-ASA is another commonly used organoarsenic feed additive potentially harmful to human health, and the environment and a possible carcinogen.[66,67] The LMOF, [Eu$_2$(clhex)·2H$_2$O)]·H$_2$O (BUC-69) was prepared via a hydrothermal reaction using EuCl$_3$·6H$_2$O reacted with 1,2,3,4,5,6-cyclohexanehexacarboxylic acid (H$_6$clhex) in deionized water and DMF (Fig. 4(A)). In this

BUC-69, the asymmetric unit includes one Eu(III) ion, three H$_2$O ligands, one clhex^{6-} linker, and one lattice H$_2$O molecule. The monomer unit is a distorted tricapped trigonal prism in which six O atoms from four clhex^{6-} and three O atoms from three different ligands, a total of nine coordination number to Eu(III). The Eu(III) ions are interconnected by protonated clhex^{6-} ligands to form a 2-D metal–organic layer and Eu(III) in these layers are further connected through deprotonated clhex^{6-} ligands in monodentate mode and an H$_2$O molecule completing a 3-D structure. The clhex^{6-} ligands exhibited an "antenna effect" which gives BUC-69 a distinct red fluorescence emission. The solid-state emission spectrum of BUC-69 consists of five sharp characteristic peaks of Eu(III) at λ = 580, 591, 616, 651, and 700 nm due to the $^5D_0 \rightarrow {}^7F_0$, $^5D_0 \rightarrow {}^7F_1$, $^5D_0 \rightarrow {}^7F_2$, $^5D_0 \rightarrow {}^7F_3$, and $^5D_0 \rightarrow {}^7F_4$ transitions, respectively (Fig. 4(B)).[68] Among them, λ = 616 nm has the highest emission intensity mostly belonging to the electric dipole transition, and produces a highly polarizable chemical environment due to $^5D_0 \rightarrow {}^7F_2$ transitions. The investigation of fluorescence emission of BUC-69 in deionized water before and after the addition of p-ASA with increasing concentrations revealed that the emission intensity of BUC-69 decreases upon the addition of p-ASA (Fig. 4(C)). BUC-69 gave a selective quenching effect for p-ASA

even in the presence of other competing metal ions and the result remains the same when the sensing studies were performed under acidic as well as alkaline conditions (Fig. 4(D)). The overlap of the absorption spectrum of *p*-ASA with the excitation spectrum of BUC-69 indicated the fluorescence quenching to be the result of radioactive energy transfer. The calculated LoD value of 1.81 μM confirms that BUC-69 can be a potential sensor for the ultra-trace sensing of *p*-ASA. The fluorescence emission remains intact even after five cycles of sensing (Fig. 4(E)). In a nutshell, BUC-69 can be a selective, sensitive, and reusable fluorescence sensor with highly desirable properties for the practical sensing of *p*-ASA in water.

A new approach of using a heterostructured MOF-on-MOF porous membrane with cascade function was fabricated and used for effective sensing of $Cr_2O_7^{2-}$ ions and *p*-ASA feed additives.[69] Inspired by the earlier studies on the incorporation of functional materials such as quantum dots,[70] nanofibers,[71] and porous polymers[72] with other functional structures, Yang *et al.* fabricated a heterostructured Cu(II)-tpt-on-Cu(I)-tpt (tpt = 5-[4(1*H*-1,2,4-triazol-1-yl)]phenyl-2*H*-tetrazole) based membrane, where Cu(I)-tpt and Cu(II)-tpt MOFs were synthesized from same ligand was integrated into a porous membrane by a layer-by-layer approach.[69] The Cu(I)-tpt MOF is a 3D framework with a *sra* network topology (Fig. 5(A)–(D)), while the Cu(II)-tpt MOF is crystalized in the ant network topology (Fig. 5(E)–(H)). The first Cu(I)-tpt layer was grown by a one-pot approach on a Cu_2O nanostructured array and the second Cu(II)-tpt layer was deposited using liquid-phase epitaxy. The integrated heterostructured MOF materials combined the performance of both Cu(I)-tpt and Cu(II)-tpt MOFs and showed an enhanced adsorption efficiency for $Cr_2O_7^{2-}$ (203.25 mg g^{-1}) and effective fluorescence sensing performance towards *p*-ASA (LoD = 0.0556 μg L^{-1}). The Cu(II)-tpt-on-Cu(I)-tpt MOF membrane itself is fluorescent (λ_{em} = 540 nm) and when $Cr_2O_7^{2-}$ was added to it, $Cr_2O_7^{2-}$ ions get adsorbed on a porous membrane resulting in fluorescence quenching responses through competitive adsorption without collapsing the framework. When *p*-ASA was used, the emission at λ_{em} = 540 nm was gradually recovered (Fig. 5(I)), which is different from other fluorescence sensors discussed in this article. The turn-on fluorescence sensing responses were also seen by visual color changes (Fig. 5(J)). Thus, this hybrid MOF selectively detects *p*-ASA *via* on–off–on sensing responses even in the presence of other potential interfering species (cations, anions, organic species, other organic arsenic acids) (Fig. 5(K)), and it can only do so after adsorbing $Cr_2O_7^{2-}$.

It was observed that the sensitivity of hybrid MOFs depends on both the amount of $Cr_2O_7^{2-}$ adsorbed and *p*-ASA concentration. If the adsorbed $Cr_2O_7^{2-}$ is more, then a high concentration of *p*-ASA is required to recover the hybrid MOF's fluorescence. Also, the effect of the ratio of Cu(I)-tpt and Cu(II)-tpt MOFs on *p*-ASA sensing was explored. When the content of Cu(II)-tpt was less and it grew unevenly on the Cu(I)-tpt layer, a higher $Cr_2O_7^{2-}$ concentration was required to completely quench the fluorescence of Cu(I)-tpt layer (3 mg L^{-1}), and it displayed a low sensitivity to *p*-ASA (LOD = 0.1068 μg L^{-1}) detection. On
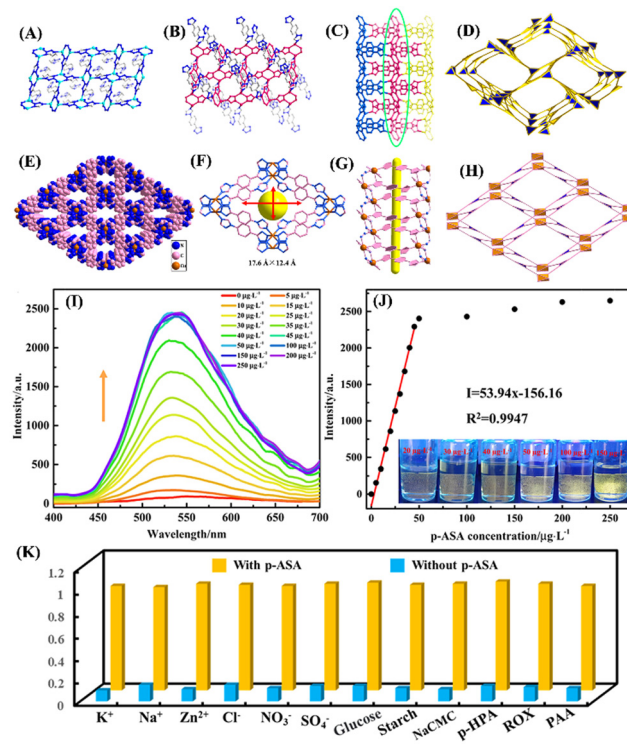

Fig. 5 (A)–(D) Crystal structure of Cu(I)-tpt; (A) coordination mode of Cu(I) with tetrazole unit of tpt ligand; (B) coordination mode of Cu(II) with triazole unit of tpt ligand; (C) 3D framework structure of Cu(I)-tpt and (D) sra network topology of Cu(I)-tpt. (E)–(H) Crystal structure of Cu(II)-tpt; (E) 3D framework structure of Cu(II)-tpt and (F) its rhombus channels of 17.6 Å × 12.4 Å; (G) 1D channels of Cu(II)-tpt; (H) ant network topology of Cu(II)-tpt; (I) the changes in fluorescence emission spectra of the Cu(II)-tpt-on-Cu(I)-tpt membrane after mixing concentration of *p*-ASA (0–200 μg L^{-1}); (J) corresponding line relationship between emission intensity at I_{540} and *p*-ASA concentrations (inset: corresponding photographs under UV lamp); (K) competitive binding ability of the Cu(II)-tpt-on-Cu(I)-tpt membrane toward various analytes. Reprinted with permission from ref. 69. Copyright 2020 American Chemical Society.

increasing the content of Cu(II)-tpt, the ratios of Cu(I)-tpt and Cu(II)-tpt were up to 2:1 and 1:1, respectively, Cu(II)-tpt grow uniformly on the Cu(I)-tpt layer and it has a higher detection sensitivity for *p*-ASA. However, when the ratio of MOFs was adjusted to 1:2, though it has higher detection sensitivity for *p*-ASA detection, its linear detection range became narrower and the correlation coefficient was poor. The optimal ratios of Cu(I)-tpt and Cu(II)-tpt in the Cu(II)-tpt-on-Cu(I)-tpt membrane are 2:1 and 1:1, respectively. Therefore, this approach of integration of adsorption with fluorescence properties makes Cu(II)-tpt-on-Cu(I)-tpt membrane a practically useful functional hybrid material for the effective detection of organoarsenic feed additives.

This strategy was further adopted by Yang *et al.* to construct the Cu(I)-tpp@ZIF-8 heterostructure and this MOF-on-MOF structure was used for efficient adsorption and sensitive detection of *p*-ASA.[73] At first the 2D MOF, Cu(I)-tpp (Htpp = 1-(4-(tetrazol-5-yl))3-(pyrzin-2-yl) pyrazol), was synthesized under solvothermal conditions. Cu(I)-tpp displayed an outstanding fluorescence emission at λ = 655 nm and possesses N-rich sites
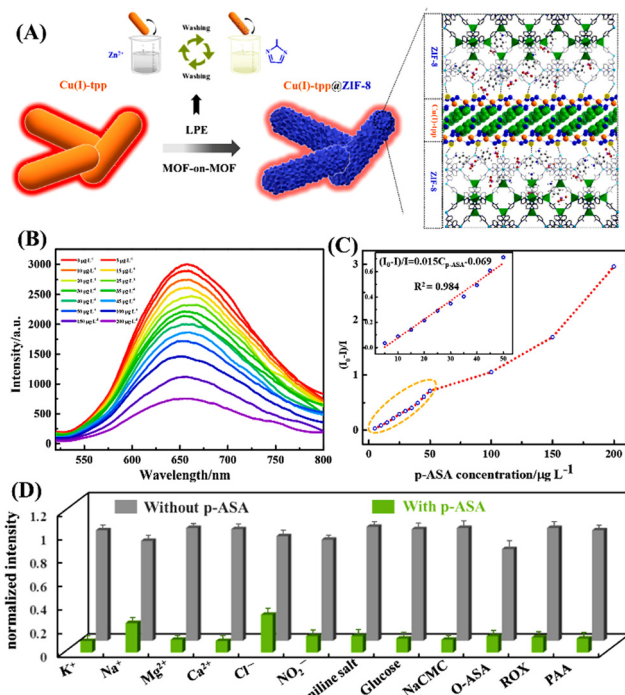
Fig. 6 (A) Schematic representation of the process of formation of Cu(I)-tpp@ZIF-8 heterostructure; (B) the changes in the fluorescence emission spectrum of Cu(I)-tpp@ZIF-8 in the presence of different concentrations of *p*-ASA (0–200 μg L^{-1}); (D) a plot of concentration *vs.* intensity ratio ($I_0 - I$)/I, (the inset is the fitment curve); (E) the selectivity plot of Cu(I)-tpp@ZIF-8 towards different interfering analytes. Reprinted with permission from ref. 73. Copyright 2022 Elsevier.

exposed on the 2D surface which makes it an excellent template for the self-assembly formation of MOF-on-MOF heterostructure. Cu(I)-tpp is used as an excellent fluorescence sensing layer and ZIF-8 is, a well-known 3D framework structure with a large surface area and excellent adsorption capacity, used as an adsorbent and sieving layer. By ignoring the lattice mismatch problem, the liquid-phase epitaxy method was adopted for the construction of Cu(I)-tpp@ZIF-8 heterostructure (Fig. 6(A)). The fluorescence 2D structure of Cu(I)-tpp was integrated with the 3D framework ZIF-8 to fabricate the target Cu(I)-tpp@ZIF-8 heterostructure, in which Cu-(I) is tightly wrapped by the ZIF-8 framework structures. Owing to the combined properties of adsorption and fluorescence sensing, Cu(I)-tpp@ZIF-8 simultaneously exhibited an appreciable adsorption capacity of q_{max} = 303 mg g^{-1} and excellent fluorescence quenching responses (LOD = 0.4 μg L^{-1}) and high selectivity for *p*-ASA in an aqueous solution (Fig. 6(B) and (C)). Notably, Cu(I)-tpp@ZIF-8 showed special sensing responses to *p*-ASA while its isomer *o*-ASA and other competing analyte ROX showed poor sensing properties (Fig. 6(D)). Therefore, the Cu(I)-tpp@ZIF-8 could be a promising sensing platform for adsorptive removal and selective sensing of *p*-ASA and thus potential materials for wastewater treatment and water quality management.

Recently, Ghosh *et. al* reported an interesting example of hydrolytically stable cationic MOF, iMOF-12C, for the precise

and sensitive detection of organoarsenic compounds such as ROX and *p*-NIT in water.[74] iMOF-12C was synthesized from an N-donor-based linker tris(4-(1*H*-imidazole-1-yl)phenyl)amine (TIPA) which was reacted under the solvothermal condition with Zn(NO$_3$)$_2$ and 1,5-naphthalenedisulfonic acid (NDSA) in water and DMF solvent mixture (see Fig. 7(A) for the structure of TIPA). The asymmetric unit of iMOF-12C includes four Zn(II) ions, four units of TIPA, three units of NDSA, one H$_2$O molecule coordinated to Zn(II) ion, and two DMF guest molecules (Fig. 7(B)). A close look at the framework structure revealed an unprecedented coordination geometry of the Zn(II) metal node. One Zn(II) metal node was of trigonal bipyramidal geometry and the other Zn(II) metal node was of tetrahedral geometry within a single framework structure. The backbone of iMOF-12C was cationic and this positive charge was balanced by two uncoordinated NDSA molecules. The framework of iMOF-12C was further stacked in an ABAB fashion to form a 1D porous channel, which was filled with NDSA molecules
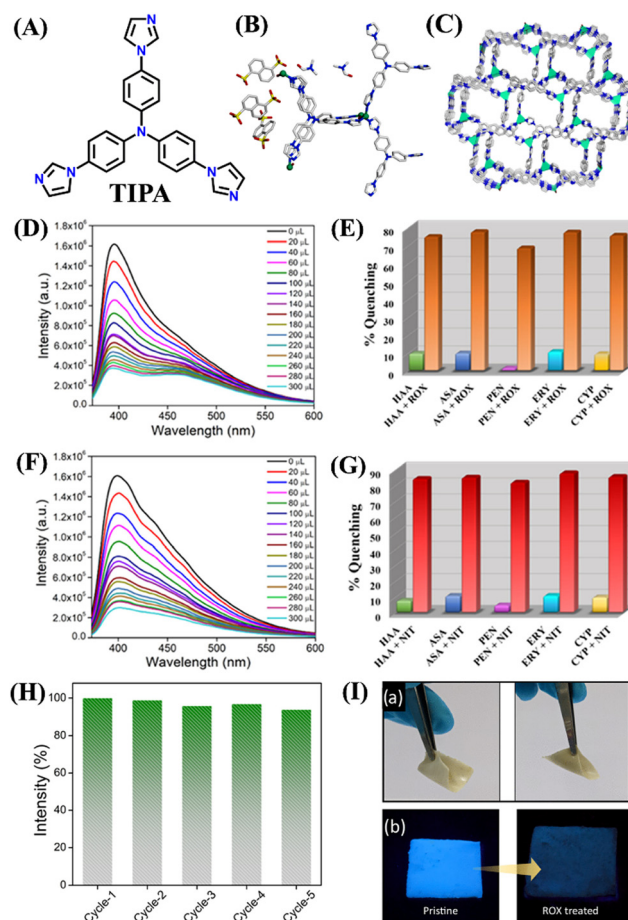

Fig. 7 (A) The structure of ligand TIPA; (B) the asymmetric unit, and (C) the framework structure of iMOF-12C with 1D porous channel; the fluorescence quenching observed after the addition of (D) ROX and (F) *p*-NIT; the selectivity graph for (E) ROX and (G) *p*-NIT; (H) reversible sensing responses of iMOF-12C toward ROX detection; (I) mixed-matrix membrane of iMOF-12C for practical sensing of ROX in water medium. Reprinted with permission from ref. 74. Copyright 2023 American Chemical Society.

(Fig. 7(C)). The cationic framework iMOF-12C exhibited photoluminescence both in the solid state and in an aqueous medium. iMOF-12C showed an intense emission peak at λ = 413 nm emanating from the ligand-to-ligand charge transfer (LLCT) and a low-energy band at λ = 435 nm was due to the ligand-to-metal charge transfer transition (LMCT). Considering the excellent photoluminescence properties and high framework stability in water, iMOF-12C was used as a promising chemosensor for the effective sensing of ROX and p-NIT in water. Upon the addition of ROX and p-NIT, the initial strong fluorescence emission of iMOF-12C was drastically quenched and the quenching efficiency was calculated to be 78% for ROX and 82% for p-NIT (Fig. 7(D) and (F)). The high fluorescence quenching efficiency for p-NIT was ascribed to its being more electron-deficient than ROX. The LOD of iMOF-12C was calculated as 3.95 ppb for ROX and 1.35 ppb for p-NIT; this level of sensitivity is much lower than the safety limit ($<$ 10 ppb) set by WHO. The Stern–Volmer quenching constant (K_{SV}) was calculated to be 1.95×10^4 M^{-1} for ROX and 2.437×10^4 M^{-1} for p-NIT. Interestingly, similar fluorescence titration studies using other organoarsenics such as p-ASA, and AA showed poor fluorescence quenching (Fig. 7(E) and (G)). Also, other potentially interfering analytes such as penicillin, erythromycin, and cypermethrin displayed almost negligible fluorescence quenching. The high selectivity of iMOF-12C toward ROX and p-NIT was due to the synergistic combinations of functional groups NO$_2$ and AsO(OH)$_2$; these functional groups were responsible for the observed enhanced fluorescence quenching of iMOF-12C. The fluorescence sensing propensity of iMOF-12C was recyclable and even after five cycles of sensing studies, the emission intensity was almost regained (Fig. 7(H)). Further, for practical application, iMOF-12C-based mixed-matrix membranes (MMM) were fabricated, and they showed excellent organoarsenic detection in water. The findings of this work highlight the potential of iMOF-12C toward real-time detection of organoarsenic feed additives in water bodies (Fig. 7(I)).

Last year, Pal et $al.$ reported a fluorescence sensor based on MOF-corn starch gel composite (1@CS) (Fig. 8(A)).[75] The composite was synthesized by the solvothermal reaction between Zn(NO$_3$)$_2$·6H$_2$O in DMF and linker 2-amino terephthalic acid (NH$_2$·BDC) and the composite was used to detect ROX in an aqueous medium. Under the excitation wavelength of λ = 365 nm, the dispersed DMF medium of 1@CS shows photoluminescence at λ = 435 nm, which signifies that the emission from 1@CS is completely ligand-based (Fig. 8(B)). The fluorescence titration studies showed a good linear fit and ROX was found to quench the fluorescence of 1@CS with a quenching efficiency of 85%, with LOD of 6.86 ppm and the Stem–Volmer constant (K_{SV}) value of 1.33×10^3 M^{-1}. 1@CS was able to detect ROX via fluorescence turn-off mode and the mechanism of such a sensing process suggested the presence of strong interaction between 1@CS and analyte through PET and FRET. Therefore, the composite 1@CS can be a promising responsive material for trace monitoring and real-field analysis of ROX in food specimens (Fig. 8(C) and (D)).

Recently, Wang et $al.$ reported an acid–base stable luminescence coordination polymer, HNU-62, for selective detection of
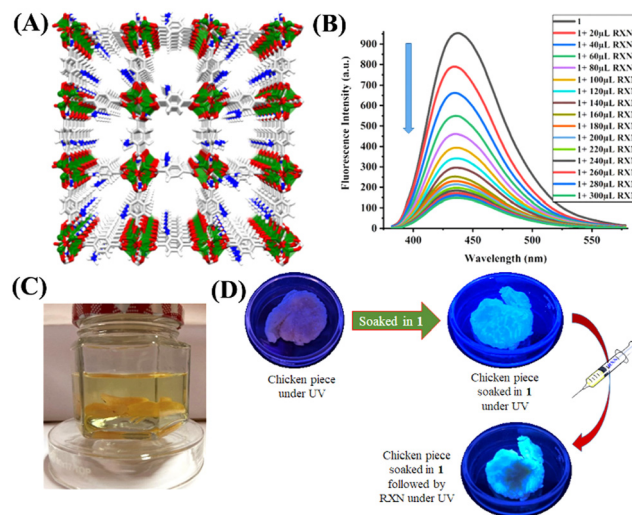

Fig. 8 (A) The 3D framework structure of luminescence Zn–MOF; (B) the changes in fluorescence emission spectra of Zn–MOF after adding increasing concentration of ROX (0–300 μL); (C) chicken piece immersed in the solution of ROX; (D) colorimetric response of the chicken piece soaked in Zn–MOF and followed by the addition of ROX. Reprinted with permission from ref. 75. Copyright 2022 American Chemical Society.

ROX in water.[76] In this work, the hydrophobic organic linker, 4-carboxytriphenylamine (HL, Fig. 9(A)), was reacted with Zn(II) ions to generate HNU-62. It was observed that the good chemical and water stability of HNU-62 in a wide range of pH is provided by the hydrophobicity of organic linkers. A white needle-shape single crystal was obtained from the reaction mixture and the diffraction analysis showed that the structure of HNU-62 consists of two Zn(II) ions and four L$^-$ linkers (Fig. 9(B)). Among two Zn(II) ions, one Zn(II) adopted a triangular bipyramid configuration and the other Zn(II) ion exhibited a square-pyramid geometry. The multifaceted coordination of HL with Zn(II) ions resulted in a 1D chain that further extended through π–π stacking between the adjacent organic ligand. HNU-62 was highly emissive and showed good sensing performances towards organoarsenics. The strong emission intensity of HNU-62 at λ = 428 nm (Φ = 8.32%) was drastically quenched with high selectivity for ROX in water (Fig. 9(C) and (D)). The mechanism of fluorescence quenching was attributed to a competitive absorption and resonance energy transfer. The sensitivity of HNU-62 for ROX was found to be 4.5×10^{-6} M. Furthermore, HNU-62 exhibited excellent selectivity and recyclability for ROX detection in real samples of pig feed (Fig. 9(E)). This study demonstrated not only the selective fluorescence sensing of ROX in real-water samples but also highlighted a new synthetic method to develop water-stable luminescence coordination polymers.

4. Covalent-organic frameworks (COFs)-based fluorescence sensor

Covalent organic frameworks (COFs) are emerging classes of crystalline porous polymers with tuneable structures and
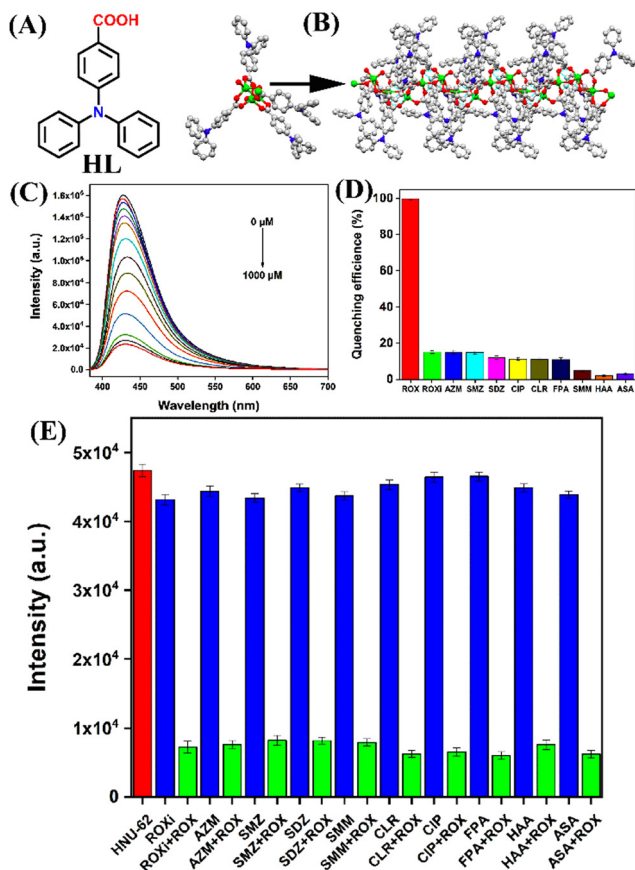
Fig. 9 (A) The structure of organic linker (HL); (B) an asymmetric unit and extended solid-state structure of HNU-62; (C) the strong fluorescence quenching observed for HNU-62 after the addition of ROX in water; (D) anti-interference plot showing a high selectivity for ROX; (E) competitive plot of sensing ROX in presence of other interfering analytes. Reprinted with permission from ref. 76. Copyright 2023 Elsevier.
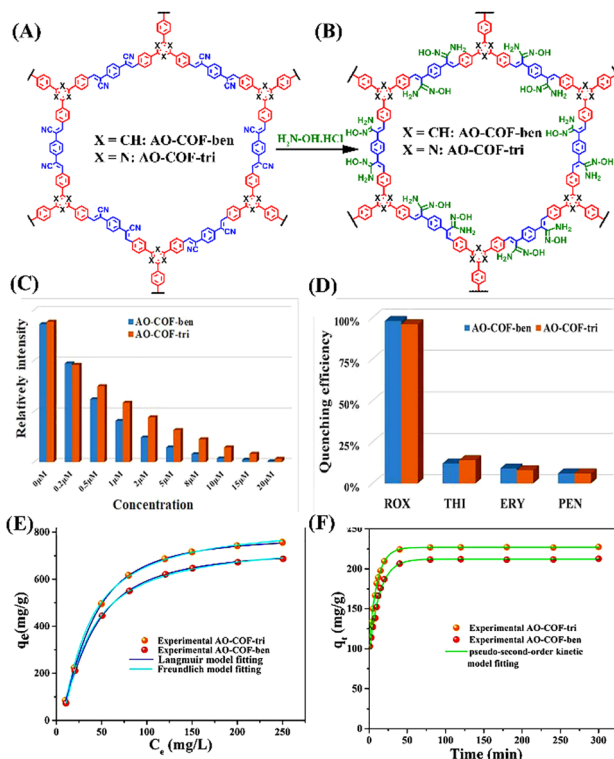

Fig. 10 The structures of functionalized COFs (A) AO-COF-ben and AO-COF-tri and (B) their post-functionalized structures; observed fluorescence changes after the addition of different concentrations of ROX to (C) AO-COF-ben and (D) AO-COF-tri; adsorption isotherms for ROX adsorption by (E) AO-COF-ben and AO-COF-tri; (F) adsorption kinetic curves of ROX by AO-COF-ben and AO-COF-tri. Reprinted with permission from ref. 80. Copyright 2022 Elsevier.

multifunctional properties.[77] In recent years, COFs have been used for various practical applications like gas adsorption and storage, catalysis, chemical sensing, and stimuli-responsive drug delivery.[78] COFs-based fluorescence materials are particularly promising for fluorescence chemosensing applications owing to their interesting photophysical characteristics and facile synthesis.[79] Last year Voort et al. developed two isoreticular 2D-amidoxime functionalized conjugated frameworks, namely AO-COF-ben and AO-COF-tri, which not only function as fluorescence sensors for detection but also as adsorbents for efficient removal of ROX feed additive from water (Fig. 10(A) and (B)).[80] In these COFs, the 2D layers are stacked in eclipse form and the framework possesses good thermal and chemical stability. The extended π-electron conjugation along the 2D network of COFs makes them exhibit strong fluorescence emission. Both the COFs, AO-COF-ben, and AO-COF-tri can selectively detect ROX in the aqueous medium even in the presence of other potentially competing organic species present in livestock-firm wastewater including p-ASA, with a quenching efficiency of 98% and 97%, respectively (Fig. 10(C) and (D)). There was no spectral overlap between the absorption spectrum

of ROX and the emission spectra of COFs and thus no FRET mechanism was involved in the fluorescence quenching processes.

Among various analytes, only the LUMO of ROX was observed to be lower in energy than that of the LUMO of COFs, implying a PET responsible for the observed fluorescence quenching; thereby these MOFs exhibit high selectivity for ROX. Since LUMO is associated with the anti-bonding orbital of the central hexagonal ring and as AO-COF-tri contains electronegative nitrogen, the electron transfer process is slower for AO-COF-tri than that of AO-COF-ben resulting in less quenching efficiency. The Stern–Volmer plot of AO-COF-ben and AO-COF-tri both fits well for ROX, with LOD value of 6.5 nM and 12.3 nM, respectively. The K_{SV} values of AO-COF-ben and AO-COF-tri towards ROX were determined as 1.35×10^4 M^{-1} and 1.05×10^4 M^{-1}, respectively. Even after 5 cycles of recyclability test, the quenching efficiency remains unchanged for both the COFs, stating its reusability. Along with the detection of ROX, due to their highly porous nature, these COFs were capable of adsorbing ROX from water. The adsorption follows Langmuir adsorption isotherm with adsorption capacity of 732 and 787 mg g^{-1} in the case of AO-COF-ben and AO-COF-tri for ROX, respectively (Fig. 10(E) and (F)). These amounts of adsorption are higher than already reported adsorbents like UIO-66,[81]

MIL-100-Fe,[82] *etc.*, and the adsorption time is also short, reaching the saturation in just 20 and 25 min for AO-COF-tri and AO-COF-ben, respectively. The interactions that are responsible for the adsorption of ROX are hydrogen bonding between ROX and the amidoxime functional groups of the COFs and π–π donor–acceptor interaction between the COFs and ROX. The greater adsorption of ROX in the case of AO-COF-tri can be attributed to its planer structure, which leads to more effective π–π stacking interactions. These results indicate that the conjugated amidoxime-functionalized COFs can be used as potential fluorescence sensors as well as polymeric adsorbents for the practical detection and removal of organoarsenic feed additives from wastewater.

5. Hydrogen-bonded organic frameworks (HOFs)-based fluorescence sensor

Hydrogen-bonded organic frameworks (HOFs) are new classes of crystalline porous organic solids constructed through hydrogen-bonded self-assembly of pre-designed organic ligands substituted with self-assembling functionalities.[83] Owing to their high surface area, porosity and tuneable pore size, and facile synthesis, HOFs have gained significant research attention and they have been used in various applications including gas adsorption and separation, chemical sensing, proton conductivity and photodynamic therapy, and so on.[84,85] Among the porous materials, HOFs have some unique properties like solution processability due to their high solubility and are thus easy to purify and recycle by a simple recrystallization process.[85] HOFs are low-density materials and their non-metallic nature makes them biocompatible for their biological applications. Fluorescence HOFs built from fluorescence organic linkers are particularly useful for their fluorescence sensing applications. In recent years, a wide variety of fluorescence HOFs have been developed and explored their fluorescence sensing applications towards various analytes.[86]

In 2020, Xiang *et al.* reported a 2-fold interpenetrated fluorescent HOF, namely HOF-22, which has been successfully obtained through hydrogen-bonding directed self-assembly of a tri-carboxylic acid, 5′-(4-carboxyphenyl)-2′,4′,6′-trimethyl-[1,1′:3′,1″-terphenyl]-4,4″-dicarboxylic acid (H_3CTTA) by simply recrystallization in ethanol (Fig. 11(A)).[87] HOF-22 was used as a fluorescent sensor for the efficient detection of two representative organoarsenics ROX and *p*-NIT in an aqueous medium. The asymmetric unit of HOF-22 contains one molecule of H_3CTTA and two ethanol guest molecules are trapped within the pores. Among three carboxylic (–COOH) groups of H_3CTTA, one is connected to the CH_3 moiety of ethanol *via* hydrogen bonding, and the other two –COOH are connected to adjacent H3CTTAs *via* hydrogen bonding resulting in a 1D zig-zag structure. This 1D structure was further connected through short interactions between the CH_3 group of ethanol and aromatic hydrogen of H_3CTTA forming a 2D network (Fig. 11(B)). These 2D networks transformed into a 3D framework through multiple
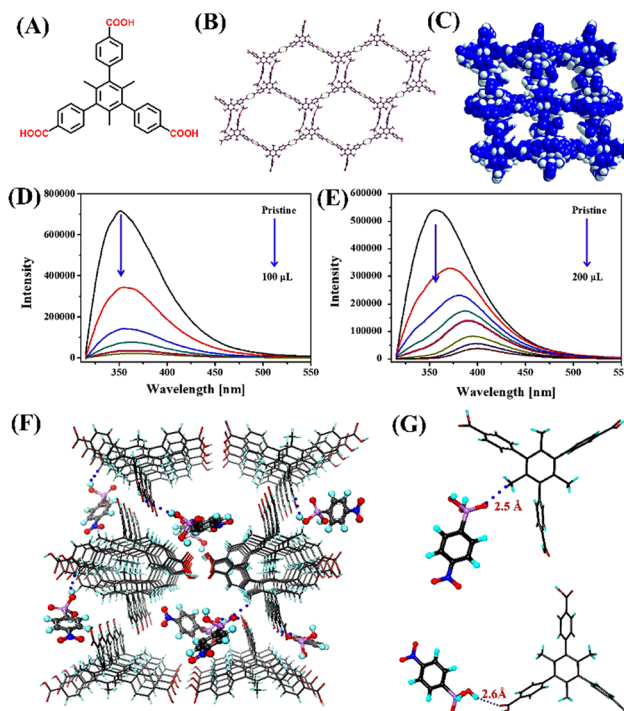

Fig. 11   (A) The structures of ligand H_3CTTA; (B) crystal structure of HOF-22 showing a 2D layer formation between adjacent chains; (C) representation of HOF-22 porous framework; the observed relative changes in fluorescence emission intensity for HOF-22 after adding (D) *p*-NIT and (E) ROX; (F) the simulated structure of *p*-NIT loaded HOF-22 and (G) selected fragments indicating the hydrogen-bonding interactions between HOF-22 and *p*-NIT. Reprinted with permission from ref. 87. Copyright 2020 Canadian Science Publishing.

intermolecular hydrogen bond-like (C–H⋯O) short interactions (Fig. 11(C)). The existence of these weak interactions was probed by simulation studies. The simulated structure of HOF-22 loaded with *p*-NIT analyte confirms the existence of two kinds of hydrogen bonding between HOF-22 and *p*-NIT molecules, which is responsible for its enhanced binding with HOF-22 and thus substantial fluorescence quenching (Fig. 11(F) and (G)). Upon excitation at 300 nm, HOF-22 dispersed in water showed strong fluorescence emission, and the emission was drastically quenched after the addition of ROX and *p*-NIT (Fig. 11(D) and (E)). The fluorescence quenching efficiency was estimated as 93% for ROX and 97% for *p*-NIT. The Stern–Volmer quenching constant was determined to be 11 800 M^{-1} for ROX and 61 500 M^{-1} for *p*-NIT. It was proposed that PET and FRET were considered as the mechanisms responsible for the observed fluorescence quenching of HOF-22. This report demonstrated the significance of luminescence HOF materials as potential fluorescence sensors for trace-level sensing of organoarsenic feed additives.

6. Fluorescence quantum dots (QDs)-based chemosensors

Fluorescence quantum dots (QDs) are very attractive and promising classes of nanomaterials with unique photophysical
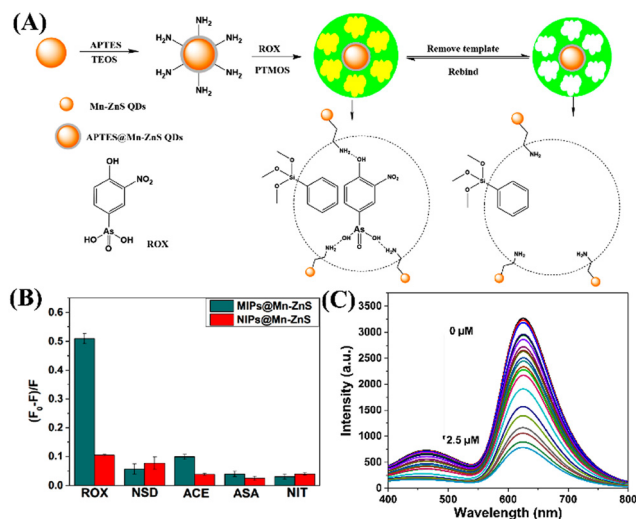
Fig. 12 (A) Schematic representation of the preparation method of MIPs@Mn–ZnS QDs for ROX sensing; (B) the relative changes in emission intensity of MIPs@Mn–ZnS QDs (red bar) in the presence of various analytes; (C) decreases in the emission intensity of MIPs@Mn–ZnS QDs upon increasing the concentration of ROX. Reprinted with permission from ref. 90. Copyright 2022 MDPI.

properties such as large Stokes shift, and narrow and symmetric emission.[88] QDs are used in biosensing applications because of their bio-compatibility, cost-effectiveness, and recyclability.[89] In 2022, Chen *et al.* particularly chose manganese-doped Zn sulphide (Mn–ZnS) QDs for ROX feed sensing.[90] The Mn–ZnS QDs are less toxic than other toxic heavy metals like Cd, and Hg-based QDs[91] and show high resistance to photo-bleaching and chemical degradation. In the design, first Mn–ZnS QDs were coated with 3-mercaptopropy trimethoxysilane (MPTS), then by silica coating to protect QDs followed by amine functionalization. It was then covered with phenyltrimethoxysilane PTMOS (monomer) and tetraethylorthosilicate (TEOS) crosslinking agent with ROX as a template (Fig. 12(A)). After the polymer was formed, the ROX template was washed off, here ROX left an imprint on the polymer surrounding the QDs. The fluorescence quenching on

molecularly imprinted polymer MIP@Mn–ZnS QDs was due to the following reason: the groups of nitro and the arsenic acid in ROX were all electron-deficient, however, the amino groups of the MIPs@Mn–ZnS QDs were electron-rich and thus, electrons could transfer from the MIPs@Mn–ZnS QDs to ROX through their strong binding to the template molecule, causing the quenching of the MIPs@Mn–ZnS QDs. The electrons were excited from the valence band to the conduction band and transited to the initial condition to generate the emissions. Therefore, the mechanism might be attributed to PET. The fluorescence quenching titration showed a very good linear fit to the Stern–Volmer plot, with a LOD of 4.34 nM for ROX (Fig. 12(C)). Also, MIPs@Mn–ZnS QDs can selectively detect ROX even in the presence of other potentially competing analytes such as 4-aminophenylarsonic acid, 2-methoxy-5-nitrophenol, 3-acetamido-4-hydroxy-phenylarsonic acid, and Nitroxinil (Fig. 12(B)). The high selectivity of MIPs@Mn–ZnS towards ROX was due to the tailor-made recognition sites matching the size, shape, and space of the template molecule. The results obtained demonstrated that MIPs@Mn–ZnS QDs could be a suitable fluorescence sensor for fast, selective, reversible, and sensitive detection of ROX even in complicated sensing samples.

7. Conclusions and outlook

In this review article, we have discussed in detail the synthesis, structure, photophysics, and fluorescence sensing properties of various fluorescence chemosensors such as MOFs, COFs, HOFs, and QDs reported to date for the effective detection of organoarsenic feed additives. The fluorescence sensors are grouped according to their structure and functional properties. Table 1 summarizes the fluorescence sensing performances of all the chemosensors discussed in this article. Interestingly, several of the fluorescence sensors exemplified herein displayed excellent fluorescence sensing performances like fast sensing responses, the ultra-trace limit of detection, and high selectivity toward organoarsenic detection in competitive

Table 1 The fluorescence sensing properties of different sensors are highlighted in this article

Sensors	λ_{max} (nm)	Sensing medium	Target analyte	LoD	K_{SV} (M^{-1})	Sensing mechanism	Ref.
BUT-18	331	H$_2$O	ROX	15.7 ppb	185 467	PET, FRET	61
			p-NIT	32.2 ppb	84 664		
BUT-19	340	H$_2$O	ROX	13.5 ppb	229 198	PET, FRET	61
			p-NIT	13.3 ppb	219 267		
BUC-69	615	H$_2$O	*p*-ASA	1.81 μM	0.0122	FRET	65
Cu(II)-tpt-on-Cu(I)-tpt	540	Aqueous solution	*p*-ASA	0.0556 μg L^{-1}	—	Redox process	69
Cu(I)-tpp@ZIF-8	655	H$_2$O	*p*-ASA	0.4 μg L^{-1}	1.5×10^4 L g^{-1}	coordination interaction	73
iMOF-12C	413	H$_2$O	ROX	3.95 ppb	1.95×10^4	PET, FRET	74
			p-NIT	1.35 ppb	2.437×10^4		
1@CS	435	DMF	ROX	6.86 ppm	1.33×10^3	PET, FRET	75
HNU-62	428	H$_2$O	ROX	4.5×10^{-6} M	7233	FRET	76
AO-COF-ben	513	Aqueous medium	ROX	6.5 nM	1.35×10^4	PET	80
AO-COF-tri	522	Aqueous medium	ROX	12.3 nm	1.05×10^4	PET	80
HOF-22	350	Aqueous solution	ROX	—	11 800	PET, FRET	87
			p-NIT		61 500		
MIP@Mn–ZnS	—	Aqueous medium	ROX	4.34 nM	68×10^4	PET	90

sensing mediums. Most of the sensors can sense organoarsenic feeds in an aqueous medium and their limit of detection is in the range of ppb level; this level of sensitivity is much lower than the allowed concentration limit which demonstrates the practical feasibility of fluorescence sensors for selective and sensitive detection of organoarsenics in wastewater. Also, the high value of K_{SV} values reported for most of the sensors indicate the strong binding affinity of sensors towards organoarsenic compounds. Owing to their encouraging properties like high porosity, large surface area, and tuneable structure and functional properties, MOFs and COFs have been considered promising sensor materials for organoarsenic detection. The porous polymeric sensors can not only sense organoarsenic compounds but also can adsorb them within their pore structures.[69]

In general, MOFs are less stable in water due to their poor hydrolytic stability; the stability can be improved by substituting organic linkers with hydrophobic functional groups, which will repel the water molecules from approaching the coordination/reactive sites. Gratifyingly, several of the fluorescence sensors discussed herein exhibit good hydrolytic stability due to their high framework stability. For instance, sensors BUT-18 and BUT-19 have good framework stability in water because the organic linkers H_3CTTA and H_3CETA are substituted with water-repelling functional groups.[61] However, the introduction of additional functional groups will block the intrinsic porosity of polymeric sensors and hence poor sensing and adsorption performances for organoarsenic compound detection. Owing to the high stability and low framework density, fluorescence COFs have become promising sensor materials for organoarsenic feed detection. The lack of solution processability is another prominent issue in designing MOFs and COFs-based practically useful sensing devices. However, this issue can be addressed by developing polymer-coated composites, which will improve the solution processability of MOFs and COFs. Therefore, the polymer-coated composites can successfully be employed as suitable sensing devices for the practical detection of organoarsenic compounds. On the other hand, given their high solubility in organic solvents, good solution processability, and easy synthesis, fluorescence HOFs-based chemosensors have been considered relevant sensors for real-time sensing organoarsenics. Due to the long-range excitonic migration, the polymer-based chemosensors such as MOFs, COFs, and HOFs showed excellent sensitivity because the mixing of trace concentration of organoarsenics can completely quench the intrinsic fluorescence emission of polymer-based sensors (*i.e.* molecular wired effect).[92]

The design and development of small-molecule-based fluorescence sensors is another emerging area of research. However, the use of small-molecule-based fluorescence sensors for practical sensing of organoarsenics is limited due to the molecular aggregate's formation in an aqueous medium. This issue can be circumvented by installing active fluorescence moieties within the extended framework structures which will inhibit the molecular aggregates formation and hence retain the intrinsic fluorescence emission emanating from active fluorophore moieties.[93] The fluorescence QDs are another type of attractive sensor material and remarkable progress has been made in the usage of QDs for sensing environmental pollutants. However, chemical instability and environmental toxicity are bottlenecks in utilizing QDs for their practical sensing applications.[94] These issues can be addressed by replacing heavy-metal QDs with organic QDs with high chemical stability and less toxicity.

In summary, in this review article, we systematically exemplified and demonstrated the fluorescence sensing properties of various kinds of fluorescence chemosensors for organoarsenic sensing in an aqueous medium. We see that there is enough room to explore further to develop practically useful sensing technologies by addressing all the limitations of existing sensor systems. We are currently working on the design and development of practically relevant polymer-based fluorescence chemosensors for selective detection and adsorption of organoarsenic feed additives from wastewater. Given the sensing performances of the examples highlighted, we believe that this review article will attract and greatly benefit readers from interdisciplinary areas of science.

Conflicts of interest

There are no conflicts to declare.

Acknowledgements

References

1 K. J. Williams, *J. R. Soc. Med.*, 2009, **102**, 343–348.
2 A. Piro, A. Tagarelli, G. Tagarelli, P. Lagonia, A. Quattrone and P. Ehrlich, *Int. Rev. Immunol.*, 2008, **27**, 1–17.
3 P. Ehrlich and A. Bertheim, Über, *Ber. Dtsch. Chem. Ges.*, 1907, **40**, 3292–3297.
4 N. F. Morehouse and O. J. Mayfield, *J. Parasitol.*, 1946, **32**, 20–24.
5 S. A. Pergantis, W. R. Cullen, D. T. Chow and G. K. Eigendor, *J. Chromatogr. A*, 1997, **764**, 211–222.
6 F. R. Gilbert, G. A. H. Wells and R. F. Gunning, *Vet. Rec.*, 1981, **109**, 158.
7 Y. S. Hong, K. H. Song and J. Y. Chung, *J. Prev. Med. Public Health*, 2014, **47**, 245–252.
8 G. Pershagen, *Environ. Health Perspect.*, 1981, **40**, 93–100.
9 M. S. Edmonds and D. H. Baker, *J. Anim. Sci.*, 1986, **63**, 533–537.
10 I. Cortinas, J. A. Field, M. Kopplin, J. R. Garbarino, A. J. Gandolfi and R. Sierra-Alvarez, *Environ. Sci. Technol.*, 2006, **40**, 2951–2957.
11 J. Meng, F. Xu, S. Yuan, Y. Mu, W. Wang and Z.-H. Hu, *Chem. Eng. J.*, 2019, **355**, 130–136.
12 K. E. Nachman, D. C. Love, P. A. Baron, A. E. Nigra, M. Murko and G. Raber, *Environ. Health Perspect.*, 2017, **125**, 363–369.
13 T. Lasky, W. Sun, A. Kadry and M. K. Hoffman, *Environ. Health Perspect.*, 2004, **112**, 18–21.
14 N. K. Mondal, *Environ. Monit. Assess.*, 2020, **192**, 590.
15 C. Directive, *Counc. Dir.*, 1999, **29**, 32.
16 U. S. Food and Drug Administration, FDA's Response to the Citizen Petition, FDA-2009-p-0594. Food Drug Adm. Silver Spring, MD 2013.
17 L. Konkel, *Environ. Health Perspect.*, 2016, **124**, A 150.

18 Y. Hu, H. Cheng, S. Tao and J. L. Schnoor, *Environ. Sci. Technol.*, 2019, **53**, 12177–12187.

19 Y. C. Liu, Y. S. Li and Z. J. Zhang, *South-to-North Water Transf. Water Sci. Technol.*, 2017, **15**, 86–93.

20 Y.-M. Liu, F.-P. Zhang, B.-Y. Jiao, J.-Y. Rao and G. Leng, *J. Chromatogr. A*, 2017, **14**, 1–9.

21 Q. Liu, H. Peng, X. Lu and X. C. Le, *Anal. Chim. Acta*, 2015, **888**, 1–9.

22 W.-X. Wang, T.-J. Yang, Z.-G. Li, T.-T. Jong and M.-R. Lee, *Anal. Chim. Acta*, 2011, **690**, 221–227.

23 A. A. Saucedo-Velez, L. Hinojosa-Reyes, M. Villanueva-Rodriguez and A. Caballero-Quintero, *Food Chem.*, 2017, **232**, 493–500.

24 X. Liu, W. Zhang, Y. Hu and H. Cheng, *Microchem. J.*, 2013, **108**, 38–45.

25 L. A. Le, A. D. Trinh, D. T. Nguyen and M. L. Bui, *Bull. Environ. Contam. Toxicol.*, 2011, **86**, 415–418.

26 P. Cava-Montesinos, M. L. Cervera, A. Pastor and M. de la Guardia, *Talanta*, 2003, **60**, 787–799.

27 L. V. Rajaković, D. D. Marković, V. N. Rajaković-Ognjanović and D. Z. Antanasijević, *Talanta*, 2012, **102**, 79–87.

28 J. Entwisle and R. Hearn, *Spectrochim. Acta, Part B*, 2006, **61**, 438–443.

29 J. F. R. Paula, R. E. S. Froes-Silva and V. S. T. Ciminelli, *Microchem. J.*, 2012, **104**, 12–16.

30 D. T. D. Qadah and J. H. Aldstadt, *Anal. Lett.*, 2018, **51**, 1321–1334.

31 B. Bouyssiere, F. Baco, L. Savary, H. Garraud, D. L. Gallup and R. Lobinski, *J. Anal. At. Spectrom.*, 2001, **16**, 1329–1332.

32 R. A. Roerdink and H. J. Aldstadt, *J. Chromatogr. A*, 2004, **1057**, 177.

33 H. Abdolmohammad-Zadeh, A. Jouyban and R. Amini, *Talanta*, 2013, **16**, 604–610.

34 B. Chen, W. T. Corns, P. B. Stockwell and J. H. Huang, *Anal. Methods*, 2014, **6**, 7554–7558.

35 H. Barros, L. M. M. Parra, L. Bennun and E. D. Greaves, *Spectrochim. Acta, Part B*, 2010, **65**, 489–492.

36 Z. L. Gang and X. J. Huang, *Trends Anal. Chem.*, 2014, **60**, 25–35.

37 K. Shrivas and K. S. Patel, *Anal. Lett.*, 2004, **37**, 333–344.

38 K. Deepa and Y. Lingappa, *Spectrochim. Acta, Part A*, 2014, **124**, 102–107.

39 J. Li, L. Chen, T. Lou and Y. Wang, *ACS Appl. Mater. Interfaces*, 2011, **3**, 3936–3941.

40 U. Kim, J. Vandergiessen and X. Savarimuthu, In Proceedings of the Global Humanitarian Technology Conference, San Jose, CA, USA, 2014, 474–478.

41 P. Li and B. Hu, *J. Chromatogr. A*, 2011, **1218**, 4779–4787.

42 T. W. Chen, U. Rajaji, S. M. Chen, S. Chinnapaiyan and R. J. Ramalingam, *Ultrason. Sonochem.*, 2019, **56**, 430–436.

43 J. R. Lakowicz, *Principles of Fluorescence Spectroscopy*, Springer, 3rd edn, 2006.

44 S. J. Bradberry, A. J. Savyasachi, M. Martinez-Calvo and T. Gunnlaugsson, *Coord. Chem. Rev.*, 2014, **273–274**, 226–241.

45 W. Guan, W. Zhou, J. Lu and C. Lu, *Chem. Soc. Rev.*, 2015, **44**, 6981–7009.

46 S. Shanmugaraju, D. Umadevi, L. M. González-Barcia, J. M. Delente, K. Byrne, W. Schmitt, G. W. Watson and T. Gunnlaugsson, *Chem. Commun.*, 2019, **55**, 12140–12143.

47 S. Shanmugaraju and P. S. Mukherjee, *Chem. Commun.*, 2015, **51**, 16014–16032.

48 M. N. B. Santos, *PhysChemComm*, 2000, **3**, 18–23.

49 X. Sun, Y. Wang and Y. Lei, *Chem. Soc. Rev.*, 2015, **44**, 8019–8061.

50 M. Chhatwal, R. Mittal, R. D. Gupta and S. K. Awasthi, *J. Mater. Chem. C*, 2018, **6**, 12142–12158.

51 B. Mohan and S. Shanmugaraju, *Dalton Trans.*, 2023, **52**, 2566–2570.

52 Y.-M. Duan, H.-W. Tian, H.-B. Li, K.-P. Wang, S. Chen, D.-S. Guo and Z.-Q. Hu, *Sens. Actuators, B*, 2023, **386**, 133757.

53 G.-H. Chen, Y.-M. Duan, Y. Li, X.-N. Han, K.-P. Wang, Z.-Q. Hu and C.-F. Chen, *Chem. Commun.*, 2023, **59**, 7431.

54 H. Furukawa, K. E. Cordova, M. O'Keeffe and O. M. Yaghi, *Science*, 2013, **341**, 1230444.

55 V. F. Samanidou and E. A. Deliyanni, *Molecules*, 2020, **25**, 960.

56 Z. Mai and D. Liu, *Cryst. Growth Des.*, 2019, **19**, 7439–7462.

57 C. Adhikari and R. Farooq, *Asian J. Chem.*, 2021, **33**, 956–962.

58 A. Halder and D. Ghoshal, *CrystEngComm*, 2018, **20**, 1322–1324.

59 P. R. Lakshmi, P. Nanjan, S. Kannan and S. Shanmugaraju, *Coord. Chem. Rev.*, 2021, **435**, 213793.

60 L. E. Kreno, K. Leong, O. K. Farha, M. Allendorf, R. P. Van Duyne and J. T. Hupp, *Chem. Rev.*, 2012, **112**, 1105–1125.

61 J. Lv, B. Wang, Y. Xie, P. Wang, L. Shu and X. Su, *Environ. Sci.: Nano*, 2019, **6**, 2759–2766.

62 Y. Cui, Y. Yue, G. Qian and B. Chen, *Chem. Rev.*, 2012, **112**, 1126–1162.

63 N. C. Burtch, H. Jasuja and K. S. Walton, *Chem. Rev.*, 2014, **114**, 10575–10612.

64 J. Canivet, A. Fateeva, Y. Guo, B. Coasne and D. Farrusseng, *Chem. Soc. Rev.*, 2014, **43**, 5594–5617.

65 C. Yang, W. Huifen, F. Peng, W. Chong and C. Wang, *Appl. Organomet. Chem.*, 2019, **33**, 1–8.

66 X. Liu, W. Zhang, Y. Hu, E. Hu, X. Xie, L. Wang and H. Cheng, *Chemosphere*, 2015, **119**, 273–281.

67 J. C. Saha, A. K. Dikshit, M. Bandyopadhyay and K. C. Saha, *Crit. Rev. Environ. Sci. Technol.*, 1999, **29**, 281–313.

68 O. Kotova, R. Daly, C. M. G. dos Santos, M. Boese, P. E. Kruger, J. J. Boland and T. Gunnlaugsson, *Angew. Chem., Int. Ed.*, 2012, **51**, 7208–7212.

69 K. Zhu, R. Fan, J. Wu, B. Wang, H. Lu and X. Zheng, *ACS Appl. Mater. Interfaces*, 2020, **12**, 58239–58251.

70 D. Zhang, Y. Xu, Q. Liu and Z. Xia, *Inorg. Chem.*, 2018, **57**, 4613–4619.

71 M. Lee, G. P. Ojha, H. J. Oh, T. Kim and H. Y. Kim, *J. Colloid Interface Sci.*, 2020, **578**, 155–163.

72 X. Yu, Y. Gong, W. Xiong, M. Li, J. Zhao and Y. Che, *Anal. Chem.*, 2019, **91**, 6967–6970.

73 K. Zhu, J. Wu, R. Fan, Y. Cao, H. Lu, B. Wang, X. Zheng, Y. Yin, P. Wang and Y. Yang, *Chem. Eng. J.*, 2022, **427**, 131483.

74 G. K. Dam, S. Fajal, S. Dutta, S. Let, A. V. Desai and S. K. Ghosh, *ACS Appl. Opt. Mater.*, 2023, **1**, 1217–1226.

75 D. B. Kanzariya, R. Goswami, D. Muthukumar, R. S. Pillai and T. K. Pal, *ACS Appl. Mater. Interfaces*, 2022, **14**, 48658–48674.

76 C. Wang, G. Ren, Q. Tan, G. Che, J. Luo, M. Li, Q. Zhou, D.-Y. Guo and Q. Pan, *Spectrochim. Acta, Part A*, 2023, **299**, 122812.

77 K. Geng, T. He, R. Liu, S. Dalapati, K. T. Tan, Z. Li, S. Tao, Y. Gong, Q. Jiang and D. Jiang, *Chem. Rev.*, 2020, **120**, 8814–8933.

78 S. Kandambeth, K. Dey and R. Banerjee, *J. Am. Chem. Soc.*, 2019, **141**, 1807–1822.

79 R. K. Sharma, P. Yadav, M. Yadav, R. Gupta, P. Rana, A. Srivastava, R. Zbořil, R. S. Varma, M. Antonietti and M. B. Gawande, *Mater. Horiz.*, 2020, **7**, 411–454.

80 H. Chen, W. Liu, L. Cheng, M. Meledina, A. Meledin, R. V. Deun, K. Leus and P. V. D. Voort, *Chem. Eng. J.*, 2022, **429**, 132162.

81 F. Ahmadijokani, H. Molavi, M. Rezakazemi, S. Tajahmadi, A. Bahi, F. Ko, T. M. Aminabhavi and J-R. Li, *Prog. Mater. Sci.*, 2022, **125**, 100904.

82 M. Liang, W. Yufang, Z. Xin, Y. Jian, X. Feng and L. Zhong, *J. Taiwan Inst. Chem. Eng.*, 2017, **70**, 74–78.

83 L. Chen, B. Zhang, L. Chen, H. Liu, Y. Hu and S. Qiao, *Mater. Adv.*, 2022, **3**, 3680–3708.

84 P. Li, M. R. Ryder and J. F. Stoddart, *Acc. Mater. Res.*, 2020, **1**, 77–87.

85 R.-B. Lin and B. Chen, *Chem*, 2022, **8**, 2114–2135.

86 C. Yang, X. Xu and B. Yan, *Inorg. Chem. Front.*, 2023, **10**, 2951–2960.

87 M. Arjmand, T. Liu, B. Wang, R. He, H. Arman, K. S. Schanze and S. Xiang, *Can. J. Chem.*, 2020, **98**, 352–357.

88 O. A. Goryacheva, C. Guhrenz, K. Schneider, N. V. Beloglazova, I. Y. Goryacheva, S. D. Saeger and N. Gaponik, *ACS Appl. Mater. Interfaces*, 2020, **12**, 24575–24584.

89 J. Weng and J. Ren, *Curr. Med. Chem.*, 2006, **13**, 897–909.

90 F. Li, J. Gao, H. Wu, Y. Li, X. He and L. Chen, *Nanomaterials*, 2022, **12**, 2997.

91 J. Geys, A. Nemmar, E. Verbeken, E. Smolders, M. Ratoi, M. F. Hoylaerts, B. Nemery and P. H. M. Hoet, *Environ. Health Perspect.*, 2008, **116**, 1607–1613.

92 A. Concellón, J. Castro-Esteban and T. M. Swager, *J. Am. Chem. Soc.*, 2023, **145**, 11420–11430.

93 W. Chen, P. Chen, G. Zhang, G. Xing, Y. Feng, Y.-W. Yang and L. Chen, *Chem. Soc. Rev.*, 2021, **50**, 11684–11714.

94 N. Tajarrod, M. K. Rofouei, M. Masteri-Farahani and R. Zadmard, *Anal. Methods*, 2016, **8**, 5911–5920.